Materials Science & Engineering A 658 (2016) 376–380

Contents lists available at ScienceDirect

Materials Science & Engineering A

journal homepage: www.elsevier.com/locate/msea

The application of Al–Ti–B preform in Al-free Mg–Zn alloy via the yttrium addition

Canfeng Fang [a,*], Guangxu Liu [a], Hai Hao [a], Linggang Meng [a], Xijun Liu [b], Xingguo Zhang [a]

[a] Key Laboratory of Solidification Control and Digital Preparation Technology (Liaoning Province), School of Materials Science and Engineering, Dalian University of Technology, Dalian 116024, China
[b] Dalian Taisheng Logistic Equipment Ltd., Dalian 116031, China

ARTICLE INFO

Article history:
Received 17 November 2015
Received in revised form
27 January 2016
Accepted 29 January 2016
Available online 30 January 2016

Keywords:
Mg–6Zn/TiB_{2p} composite
Yttrium
Microstructure
Texture
Mechanical properties

ABSTRACT

For the application of the Al–Ti–B system in Al-free Mg alloys, yttrium was selected and its effect on microstructure, texture and mechanical properties of Mg–6Zn/TiB_{2p} composite was studied. The results indicate that the addition of Y could transform the extra Al (which is the by-product of the Al–Ti–B SHS reaction) into Al_2Y and $Al_{11}Y_3$ phases, and then refined the as-homogenized microstructure of the Mg–6Zn/TiB_{2p} composite. The Al_2Y and $Al_{11}Y_3$ particles, as well as the TiB_2 particles, effectively stimulate the occurrence of dynamic recrystallization during the cross-rolling, which contribute to the grain refinement and the formation of a weak double peak texture. That results in the comprehensive improvement of the mechanical properties.

1. Introduction

Magnesium matrix composites (MMCs) have obvious advantages in specific strength, micro-hardness and wear resistance compared with magnesium alloys. In recent years, many attentions have been paid to research and develop MMCs for their promising applications in weight critical applications, especially in aerospace and automotive industries [1–5]. Due to the relative simple preparation technology and isotropic properties, particle-reinforced MMCs (i.e. PMMCs) has become an important research direction. Conventionally, the reinforced particles are usually introduced by ex-situ methods, in which the scale of the reinforcement is limited by the starting particle size and the matrix-reinforcement interface is not very clean. Fortunately, these drawbacks can be improved by in-situ techniques [6–8], such as self-propagating high-temperature synthesis (SHS), which has attracted significant interests during the last decade. Especially, Wang et al. [6] developed a new method of PMMCs preparation, in which the TiB_2 reinforcements were in-situ synthesized by using high temperature of molten magnesium to ignite an Al–Ti–B preform. This solved the key problems, i.e. the introduction of the in-situ particle into matrix and the interface contamination etc. However, as a by-product, Al is inevitable in the SHS reaction, which will restrict the application of Al–Ti–B system in Al-free magnesium alloys, such as Mg–Zn series.

Recently, Al_2Y intermetallic compound with high melting temperature (1748 K), high Young's modulus (158 GPa) and high hardness (HV=645) has attracted lots of attentions [9]. More importantly, the Al_2Y phases can be formed by the in-situ reaction between Al and Y elements in the molten magnesium alloys and act as effective heterogeneous nucleation sites for α-Mg [10–12]. Qiu et al. [10] reported that an addition of 0.6–1.0 wt% Al into the Mg-10 wt% Y melt promoted the in-situ formation of Al_2Y, which reduced the average grain size from 180 to 36 μm. Zhao et al. [11] investigated the influence of Y on AZ91D alloys and their results showed that the addition of Y led to the precipitation of rod-shaped Al_2Y phase and exerted a favorable influence on reducing grain size of the AZ91D alloy in both as-cast and extruded states. Tensile tests confirmed that the ultimate tensile strength, yield strength and elongation of the as-cast and extruded AZ91D alloys increase significantly with increasing content of Y. Similarly, reports by Cui et al. [12] showed that adding Y to the Mg–5Li–3Al–2Zn alloy also resulted in the formation of Al_2Y compound and caused grain refinement of the matrix. The tensile strength and ductility reach peak values when the Y additions are 0.8 wt% and 1.2 wt%, respectively.

Accordingly, the addition of Y can consume the residual Al generated by the Al–Ti–B SHS reaction, which provides a positive access for the use of Al–Ti–B SHS system in Al-free magnesium alloys. In the present work, in-situ Mg–6Zn/TiB_{2p} composites with and without Y addition were prepared by stir casting assisted with ultrasonic vibration and then followed by cross-rolling. The

* Corresponding author.
E-mail address: fcf@dlut.edu.cn (C. Fang).

http://dx.doi.org/10.1016/j.msea.2016.01.112
0921-5093/

influence of Y element on the microstructure, texture and mechanical properties of the Mg–6Zn/TiB_{2p} composites is carefully investigated in this work.

2. Experimental procedure

The Al–Ti–B SHS preforms were made with the commercial powders of aluminum, titanium and boracium, in which the atomic ratio of titanium and boracium approximated to the stoichiometry of TiB_2 and the mass ratio of aluminum was 50%. The mean diameters of aluminum, titanium and boracium powders were 29, 30 and 2 μm respectively. Powder blend was firstly mixed in a high energy ball miller for 8 h with a speed of 300 r/min and ball-to-powder ratio of 10:1, and then cold pressed at pressure of 30 MPa into a cylindrical preform (35 mm in diameter).

An Al-free magnesium alloy with a nominal composition of Mg–6Zn (wt%) was used as the starting matrix material. The Mg–6Zn matrix alloy was firstly melted at 720 °C in a stainless steel crucible placed in an electric resistance furnace under an anti-oxidizing flux. As the temperature of melt increased to about 760 °C, about 4 wt% Al–Ti–B preform preheated at 300 °C for 2 h was added and SHS reaction then occurred as reported in the Ref. [6]. After the SHS reaction completed in the molten Mg–6Zn alloy, about 3.5 wt%Y was added in the form of Mg–Y master alloy. When the entire Mg–Y master alloy was melted, the molten composite was cooled to 620 °C and mechanically stirred to break the products of SHS. After that, the melt was reheated to 700 °C and then ultrasonically processed at 600 W power level for 20 min. At last, the composite melt was elevated to a pouring temperature of 720 °C and cast into a steel mould which brushed with 30% talc water glass solution and preheated at 300 °C. For comparison, Mg–6Zn/TiB_{2p} composite without Y addition was also cast under the same conditions.

The samples were homogenized at 345 °C for 24 h and machined into rectangular shape with dimension of $100 \times 80 \times 18$ mm^3. Before hot-rolling, the samples were preheated at the temperature of 340 °C for 30 min. Cross-rolling where each rolling direction changes at 90° (Fig. 1) was conducted at 340 °C. After each rolling pass, the rolled samples were reheated to the rolling temperature. Finally, a total plastic deformation of 70% was reached, and then the rolled sheets were subjected to air cooling.

The chemical compositions of the prepared composites were analyzed by X-ray fluorescence (XRF, XRF-1800) analyzer, as shown in Table 1. The phase analysis and macro-texture test were performed by an X-ray diffractometer (XRD, Empyrean) with Cu *K*a radiation. Energy dispersive X-ray spectroscopy (EDS) was also used to determine the phases formed in the samples. The microstructure observations were carried out by optical microscope (OM, Leica MEF4) and scanning electron microscope (SEM, SUPRA55). The specimens for the OM and SEM observation were mechanically polished and etched in the acetic picral (2.1 g picric acid + 5 ml acetic acid + 5 ml water + 35 ml ethanol). The average grain size of each composite before and after rolling was obtained by using the mean linear intercept method [13,14]. Each material used for repeat tensile tests was cut into three samples with their long axes parallel to the RD1. The tensile test was carried out with a strain rate of 1×10^{-3} s^{-1} by DNS100 universal tensile testing machine.

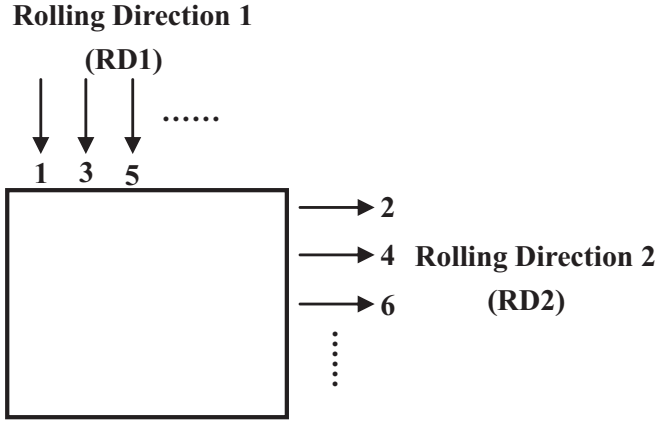

Fig. 1. The schematic diagram of the cross-rolling.

Table 1
Designation and chemical composition of the two studied composites.

Designation	Nominal composition (wt%)	Composition (wt%)				
		Zn	Al	Ti	Y	Mg
Composite A	Mg–6Zn–4(Al–Ti–B)	5.89	1.82	1.29	–	Bal.
Composite B	Mg–6Zn–4(Al–Ti–B)–3.5Y	5.92	1.96	1.33	3.36	Bal.

3. Results and discussions

3.1. Microstructures

The XRD patterns of the two studied as-homogenized composites are presented in Fig. 2. XRD analysis shows that the Mg–6Zn/TiB_{2p} composite (labeled as Composite A) is mainly composed of α-Mg and TiB_2 phase, where Al- or Zn-containing phases are not detected. It is worth noting that the additional diffraction peaks of Al_2Y and $Al_{11}Y_3$ phases emerge in the Composite B.

Metallographic characteristics of the α-Mg and reinforcement particles in the as-homogenized Composite A are clearly presented in Fig. 3. The average grain size of α-Mg is about 102 μm. According to the EDS analysis result of point A in Fig. 3b (Table 2), the particle clusters with a pretty large size consist of TiB_2 particles which are one of Al–Ti–B SHS reaction products.

Microstructures of Mg–6Zn/TiB_{2p} composite with Y addition are given in Fig. 4. It is noted that plenty of polygon particles (white arrows in Fig. 4a) and costate-shaped phases (Fig. 4b) can be

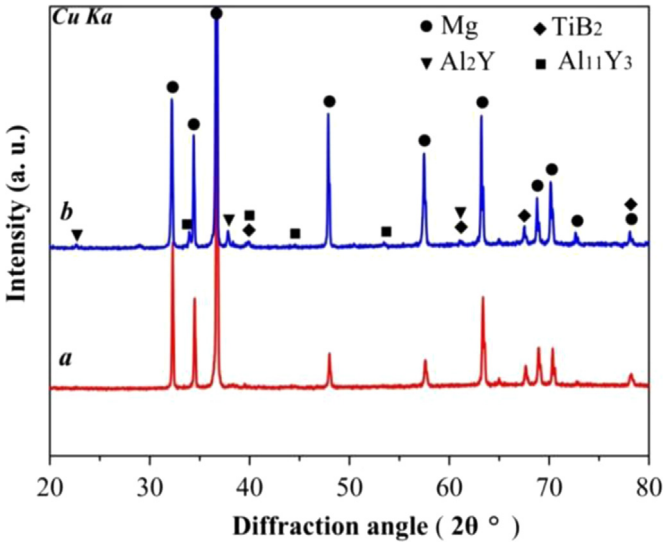

Fig. 2. XRD patterns of Composite A (a) and Composite B (b).

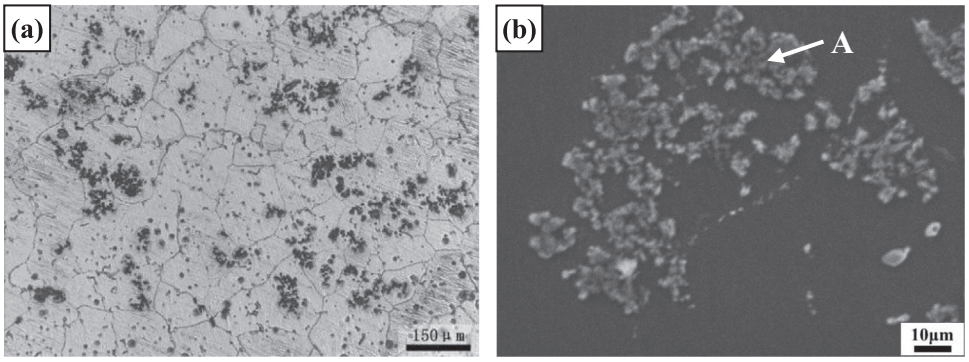

Fig. 3. The optical micrograph (a) and SEM image (b) for Composite A after homogenization treatment.

Table 2
EDS elemental analysis of the phases in the studied composites marked A, B, and C in the Figs. 3 and 4.

Point	Composition (at%)				
	Mg	Al	Ti	Zn	Y
A	77.56	10.52	9.82	2.11	–
B	2.35	58.66	–	1.27	37.71
C	84.63	9.71	–	2.52	3.15

observed. The polygon particles emerge inside the grains, while the costate-shaped phases grow from the boundary to the inner grains of α-Mg. Obviously, the precipitation of the two phases changes the solidification behavior of the Mg–Zn/TiB_{2p} composite, which results in a considerable grain refinement (~80 μm for the Composite B). In addition, there is also a reduction in the size of TiB_2 particle clusters (from ~50 μm to ~20 μm). EDS analysis for the polygon particles and costate-shaped phases (point B and point C in Fig. 4b) indicates that the atomic ratio of Al to Y is close to 2:1 and 11:3, respectively, as shown in Table 2. Combining the results of XRD pattern (Fig. 2), the polygon particle should be Al_2Y and the costate-shaped phase is $Al_{11}Y_3$.

The addition of Al–Ti–B preform leads to the formation of in-situ TiB_2 particles in the Composite A by the SHS reaction. Wang et al. [6] suggested that the incomplete reaction in the Al–Ti–B preform takes place as follows:

$$(x + 3)Al + 2Ti + 2B \rightarrow TiB_2 + TiAl_3 + xAl \quad (1)$$

In our present study, it is difficult to find the existence of $TiAl_3$ phase. Hence, the real reaction occurred in Al–Ti–B preform should be:

$$Al+Ti + 2B \rightarrow TiB_2 + Al \quad (2)$$

During the solidification, most of the in-situ TiB_2 particles were pushed forward by liquid–solid interface [14], these particles thus have a strong clustering tendency in the intergranular regions, a normal phenomenon for MMCs fabricated especially by conventional stir casting method. It is worth mentioning that Al in the preform is retained after the SHS reaction, which is not expected in the composition design of Al-free Mg–Zn matrix composite. Therefore, the addition of 3.5 wt% (1.03 at%) Y in our present work is hoped to consume the 2 wt% (1.94 at%) residual Al by the eutectic reaction between Al and Y [15]:

$$2Al + Y \rightarrow Al_2Y \quad (3)$$

However, from Figs. 2 and 4, another peritectic reaction [16] (Reaction (4)) also occurs under the disequilibrium thermodynamic conditions in addition to the eutectic reaction.

$$3Al_2Y + L \rightarrow Al_{11}Y_3 \quad (4)$$

Although the presence of $Al_{11}Y_3$ phase is out of the original expectation, it still succeeds to eliminate the residual Al by the addition of Y. Al_2Y particle whose interatomic spacing misfit with Mg matrix is less than 2% has strong potential to act as effective grain refiner for cast Mg alloys [17]. Furthermore, the costate-shaped $Al_{11}Y_3$ phases can play a role in limiting the growth of α-Mg [16]. As a result, the addition of Y succeeds in refining the microstructures of Mg–6Zn/TiB_{2p} composites to some degree.

The OM and SEM images of the two studied composites after the cross-rolling are shown in Fig. 5. Compared with the as-homogenized ones (Figs. 3 and 4), much finer equiaxed grains with well-defined boundaries can be found in Fig. 5a and b, which indicates that dynamic recrystallization (DRX) took place during the cross-rolling process [18]. Because of the rolling deformation, the large TiB_2 particle clusters which initially present in the as-cast microstructures are elongated to form TiB_2 particle streams and distributed more uniformly in the matrix. Moreover, the $Al_{11}Y_3$ phases emerged in Fig. 4b are broken into small (~3 μm in length) rod-like pieces and distributed along the rolling direction, while

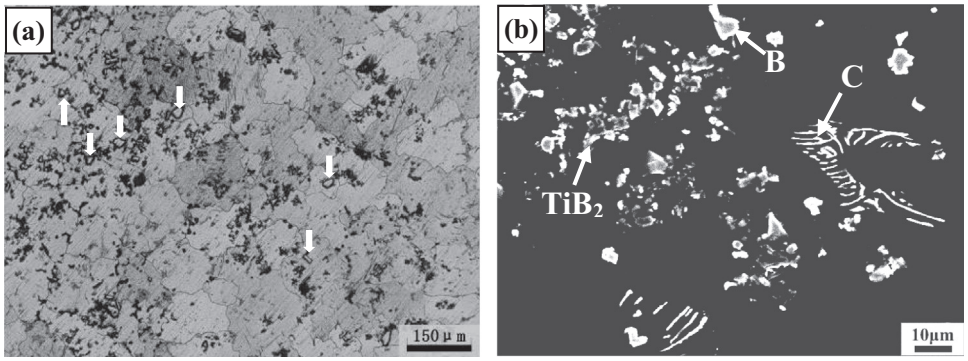

Fig. 4. The optical micrograph (a) and SEM image (b) for Composite B after homogenization treatment.

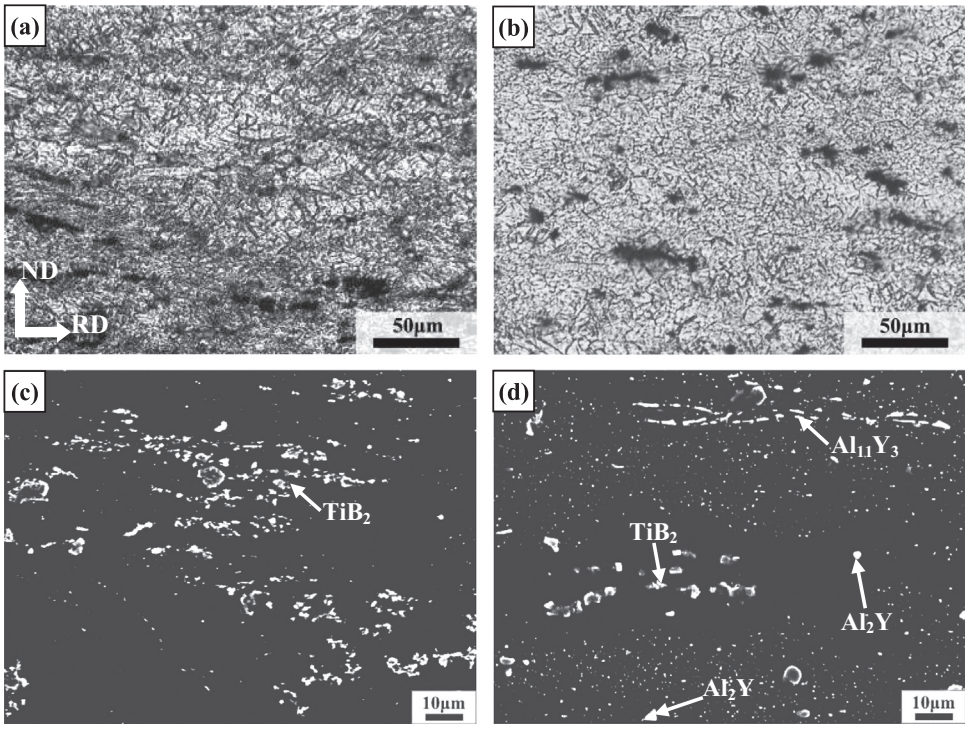

Fig. 5. Optical micrographs and SEM images of the as-rolled specimens, (a)/(c) Composites A; (b)/(d) Composites B.

no difference in the morphology of Al_2Y particles can be found before and after rolling process. It is well known that large particles (>1 μm diameter) can act as nucleation sites for DRX during hot deformation (particle stimulated nucleation or PSN) [19]. In Composite B, both Al_2Y and the broken $Al_{11}Y_3$ particles can induce the DRX of the magnesium matrix through PSN mechanism. Besides, the TiB_2 particles with smaller cluster size and more uniform distribution are better for promoting DRX. So the DRX nucleation effect of Composite B is stronger than that of Composite A, which is verified by the grain size measurements (11 μm for the Composite A and 6μm for the Composite B). Similar results were also reported in Refs. [14,20]. The small quantity of twins observed in the Composite A is further reduced in the Composite B with Y addition. This phenomenon can be related to the effect of grain refinement that is available for depressing the activity of twinning and promoting additional deformation mechanisms, such as grain boundary sliding [21].

3.2. Texture

Fig. 6 displays the texture of the two composite sheets by means of the (0002) pole figures. It can be seen that, after the cross-rolling with a 70% reduction, a basal-type texture is already formed in Composite A (Fig. 6a). Two main changes take place with the addition of Y. First, the formation of a double peak texture, in which the maxima are rotated away from the ND towards the RD2, as shown in Fig. 6b; second, the weakening of the maximum pole intensity (reduced from 9.5 to 7.5).

As described above, there is little twinning activity and furthermore it seems to be decreased with the addition of Y. Therefore, a more reasonable mechanism of double peak texture is the increasing activity of non-basal $<c+a>$ slip instead of twinning according to the views by S.R. Agnew et al. [22]. In the microstructure of Composite B, the presence of TiB_2, Al_2Y and $Al_{11}Y_3$ particles increases the total particle volume fraction, which changes the behavior of DRX accordingly. The random texture may be ascribed to the increased volume fraction of reinforced particles, as the relationship between the maximum value of the

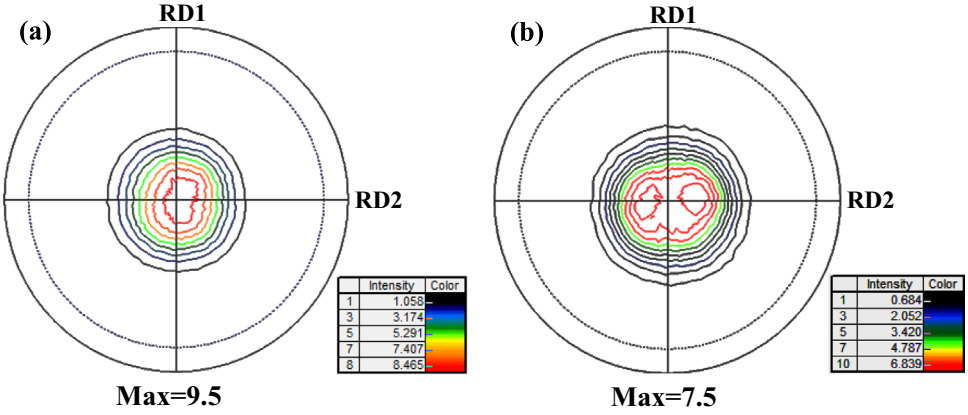

Fig. 6. (0002) pole figures tested on the RD1-RD2 plane of the as-rolled specimens, (a) Composites A, (b) Composites B.

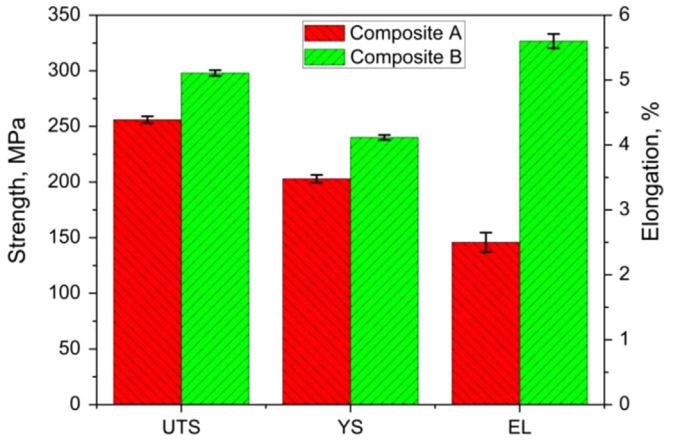

Fig. 7. Tensile properties of the as-rolled composites.

texture intensity and $Mg_3Zn_3Er_2$ particle volume fraction in the report of Wang et al. [20].

Furthermore, it has been reported in many RE/Y elements containing Mg alloys that the angular distribution of basal poles is significantly broader toward transverse direction, TD, rather than in the rolling direction, RD [21,23]. However, a spread in the basal pole towards rolling directions (RD1 and RD2) is apparent after the cross-rolling. This appearance of the pole figure should be ascribed to the 90°-directional transformation rolling in the cross-rolling. In other words, the RD2 could be considered as the TD in conventional rolling process as rolling along RD1 and vice versa.

3.3. Mechanical properties

The tensile properties of the as-rolled composites are given in Fig. 7. Compared with the as-rolled Composite A, the ultimate tensile strength (UTS) and yield strength (YS) of the Composites B increase about 40 MPa. The diffusive TiB_2, Al_2Y and $Al_{11}Y_3$ in composite matrix can pin up the dislocations and contribute dispersion strengthening to the composite, resulting in the increase of UTS of the Composite B. The YS of metal depends on its grain size, which can be described by the Hall–Petch relation: $\sigma_{ys} = \sigma_0 + kd^{-1/2}$, where σ_{ys} is the YS of the composites, σ_0 and k are experimentally derived constants and d is the average grain diameter [24]. According to the measurements of grain size in Fig. 5, there is a decrease trend in the grain size from the as-rolled Composite A to Composite B. Therefore, the YS of the Composite B is increased. Interestingly, although the strengths of Composite B are improved, its tensile elongation (EL) of 5.6% is considerably larger than that of the Composite A (2.5%). In fact, not only the grain refinement [2,5,20,25–28], but also the weakening of texture intensity [2,20,25,26] can act as ductility enhancer. Consequently, it is much reasonable that the ductility of Composite B is increased instead of decreased. Both the weakening of the texture and the improvement of elongation in tensile tests indicate a better formability of Mg–6Zn/TiB_{2p} composite modified with Y.

4. Conclusions

In this study, the Mg–6Zn/TiB_{2p} composite was prepared by the SHS method and Y was added to eliminate the by-product, i.e. Al, in the melt. After that, the evolutions of the microstructure, texture and mechanical properties of Mg–6Zn/TiB_{2p} composite were investigated. The main conclusions are summarized as follows:

1. By the formation of Al_2Y and $Al_{11}Y_3$ phases, the addition of Y consumed the residual Al, which expanded the application of Al–Ti–B SHS system in Al-free Mg alloys, and reduced the cluster size of TiB_2 particles and refined the as-homogenized microstructure of the composites.
2. The Al_2Y and $Al_{11}Y_3$ phases, as well as the TiB_2 particles, worked as nucleation sites for the dynamic recrystallization (DRX) via particle stimulated nucleation (PSN) mechanism in the cross-rolling process, which contributed to the finer microstructure and the formation of a weaker double peak texture. In addition, strength and elongation of Mg–6Zn/TiB_{2p} composite were improved simultaneously after the addition of Y.

Acknowledgments

The authors gratefully acknowledge the financial support provided by the National Natural Science Foundation of China (No. 51374047), Foundation of Liaoning Educational Committee of China (No. L2013031), and Fundamental Research Funds for the Central University (Nos. DUT15ZD201, DUT14RC (3) 134 and DUT15JJ (G) 01).

References

[1] S.S. Zhou, K.K. Deng, J.C. Li, K.B. Nie, F.J. Xu, H.F. Zhou, J.F. Fan, Mater. Des. 64 (2014) 177–184.
[2] K.S. Tun, P. Jayaramanavar, Q.B. Nguyen, J. Chan, R. Kwok, M. Gupta, Mater. Sci. Technol. 28 (2012) 582–588.
[3] H. Choi, N.A. Baena, S. Nimityongskul, M. Jones, T. Wood, M. Sahoo, R. Lakes, S. Kou, X.C. Li, J. Mater. Sci. 46 (2011) 2991–2997.
[4] A. Das, S.P. Harimkar, J. Mater. Sci. Technol. 30 (2014) 1059–1070.
[5] Q.B. Nguyen, K.S. Tun, J. Chan, R. Kwok, J.V.M. Kuma, T.H. Phung, M. Gupta, Mater. Sci. Technol. 28 (2012) 227–233.
[6] H.Y. Wang, Q.C. Jiang, Y.G. Zhao, F. Zhao, J. Alloy. Compd. 379 (2004) L4–L7.
[7] X.Q. Zhang, H.W. Wang, L.H. Liao, X.Y. Teng, N.H. Ma, Mater. Lett. 59 (2005) 2105–2109.
[8] W. Cao, C.F. Zhang, T.X. Fan, D. Zhang, Mater. Sci. Eng. A 496 (2008) 242–246.
[9] G.Q. Wu, Z.H. Ling, X. Zhang, S.J. Wang, T. Zhang, Z. Huang, J. Alloy. Compd. 507 (2010) 137–141.
[10] D. Qiu, M.X. Zhang, J.A. Taylor, P.M. Kelly, Acta Mater. 57 (2009) 3052–3059.
[11] Z.D. Zhao, Q. Chen, Y.B. Wang, D.Y. Shu, Mater. Sci. Eng. A 515 (2009) 152–161.
[12] C.L. Cui, L.B. Wu, R.Z. Wu, J.H. Zhang, M.L. Zhang, J. Alloy. Compd. 509 (2011) 9045–9049.
[13] K.B. Nie, X.J. Wang, K. Wu, X.S. Hu, M.Y. Zheng, Mater. Sci. Eng. A 540 (2012) 123–129.
[14] M.J. Shen, X.J. Wang, C.D. Li, M.F. Zhang, X.S. Hu, M.Y. Zheng, K. Wu, Mater. Des. 54 (2014) 436–442.
[15] D. Qiu, M.X. Zhang, J. Alloy. Compd. 488 (2009) 260–264.
[16] H.H. Zou, X.Q. Zeng, C.Q. Zhai, W.J. Ding, Mater. Sci. Eng. A 402 (2005) 142–148.
[17] D. Qiu, M.X. Zhang, J. Alloy. Compd. 586 (2014) 39–44.
[18] J.D. Robson, D.T. Henry, B. Davis, Acta Mater. 57 (2009) 2739–2747.
[19] S.H. Park, J.G. Jung, Y.M. Kim, B.S. You, Mater. Lett. 139 (2015) 35–38.
[20] Q.F. Wang, K. Liu, Z.H. Wang, S.B. Li, W.B. Du, J. Alloy. Compd. 602 (2014) 32–39.
[21] J. Hirsch, T.A. Samman, Acta Mater. 61 (2013) 818–843.
[22] S.R. Agnew, M.H. Yoo, C.N. Tome, Acta Mater. 49 (2001) 4277–4289.
[23] J. Bohlen, M.R. Nürnberg, J.W. Senn, D. Letzig, S.R. Agnew, Acta Mater. 55 (2007) 2101–2112.
[24] B. Zhang, X.D. Peng, Y. Ma, Y.M. Li, Y.Q. Yu, G.B. Wei, Mater. Sci. Technol. 31 (2015) 1035–1041.
[25] S. Sankaranarayanan, M.K. Habibi, S. Jayalakshmi, K.J. Ai, A. Almajid, M. Gupta, Mater. Sci. Technol. 31 (2015) 1122–1130.
[26] M. Kaseem, B.K. Chung, H.W. Yang, K.B. Hamad, Y.G. Ko, J. Mater. Sci. Technol. 31 (2015) 498–503.
[27] S.F. Hassan, M. Gupta, Mater. Sci. Eng. A 392 (2005) 163–168.
[28] S. Sankaranarayanan, R.K. Sabat, S. Jayalakshmi, S. Suwas, M. Gupta, Mater. Des. 56 (2014) 428–436.